Identification of a new isomeric state in ^{76}Zn following the β decay of ^{76}Cu

A. Chester,[1,*] B. A. Brown,[1,2] S. P. Burcher,[3] M. P. Carpenter,[4] J. J. Carroll,[5] C. J. Chiara,[5] P. A. Copp,[4] B. P. Crider,[6] J. T. Harke,[3] D. E. M. Hoff,[3] K. Kolos,[3] S. N. Liddick,[1,7] B. Longfellow,[1,2,†] M. J. Mogannam,[1,7] T. H. Ogunbeku,[6] C. J. Prokop,[8] D. Rhodes,[1,2] A. L. Richard,[1,†] O. A. Shehu,[6] A. S. Tamashiro,[9] R. Unz,[6] and Y. Xiao[1,6,‡]

[1]*National Superconducting Cyclotron Laboratory, Michigan State University, East Lansing, Michigan 48824, USA*

[2]*Department of Physics and Astronomy, Michigan State University, East Lansing, Michigan 48824, USA*

[3]*Lawrence Livermore National Laboratory, Livermore, California 94550, USA*

[4]*Argonne National Laboratory, Argonne, Illinois 60439, USA*

[5]*DEVCOM/Army Research Laboratory, Adelphi, Maryland 20783, USA*

[6]*Department of Physics and Astronomy, Mississippi State University, Mississippi State, Mississippi 39762, USA*

[7]*Department of Chemistry, Michigan State University, East Lansing, Michigan 48824, USA*

[8]*Los Alamos National Laboratory, Los Alamos, New Mexico 87545, USA*

[9]*School of Nuclear Science and Engineering, Oregon State University, Corvalis, Oregon 97331, USA*

(Received 19 July 2021; accepted 7 October 2021; published 24 November 2021)

Background: The evolution of nuclear shell structure far from stability can be explored by identifying and measuring the properties of isomers. Neutron-rich nuclei between the $Z = 28$ and the $Z = 50$ closed shells have been the subject of recent studies which have identified a number of 0.1–10 μs isomers and measured detailed spectroscopic properties.

Purpose: The purpose of this analysis was to identify and measure the properties of short-lived isomeric states populated following β decay in $Z \approx 30$, $N \approx 50$ nuclei near the doubly magic nucleus ^{78}Ni.

Methods: Radioactive ions produced by beam fragmentation at the National Superconducting Cyclotron Laboratory were implanted into a $CeBr_3$ scintillator coupled to a pixelated photomultiplier tube. Ancillary arrays of HPGe clover and $LaBr_3$ detectors were positioned around the implantation detector to measure β-delayed γ rays.

Results: The previously observed 2634-keV level in ^{76}Zn, populated following the β decay of ^{76}Cu, was identified as isomeric with a half-life of 25.4(4) ns. A combination of timing and γ-ray spectroscopy was used to confirm this assignment. Shell-model calculations were performed and indicate that this state may be a negative-parity state formed by the occupation of the $\nu 0g_{9/2}$ orbital.

Conclusions: A new isomeric state in ^{76}Zn has been identified, and its half-life was measured. Ambiguity about the structure of this state could be resolved with further experiments.

DOI: 10.1103/PhysRevC.104.054314

I. INTRODUCTION

Nuclear isomers are a useful laboratory tool to study shell evolution because of their sensitivity to changes in nuclear structure. For example, the occupancy of the $\nu 0g_{9/2}$ orbital in neutron-rich Ni and Zn isotopes gives rise to the seniority isomers ^{70}Ni^m [1], ^{76}Ni^m [2], and ^{78}Zn^m [3]. The unexpected disappearance of analogous seniority isomers in the midshell nuclei ^{72,74}Ni [4] provides additional insight into the microscopic structure of the Ni isotopes as proton excitations across the $Z = 28$ shell gap cause nearly degenerate nonisomeric excited states with different $\nu 0g_{9/2}$ configurations to become yrast [4,5]. Shell effects leading to low-lying intruder states can also cause isomerism, such as in ^{67}Co where a deformed intruder configuration is nearly degenerate with the ground state predicted by the spherical shell model [6]. Isomerism driven by complex nuclear structure effects has been observed in ^{70}Cu where three β-decaying isomeric states have been identified which arise due to a combination of one-proton, one-neutron interactions, and neutron two-particle two-hole excitations across the $N = 40$ shell gap [7]. Shape isomerism where nearly degenerate states with different shapes exist within the same nucleus has also been observed along the Ni isotopic chain [8–12] as well as in the nearby neutron-rich Mn isotopes [13].

Large-scale survey experiments have identified a number of isomers in the vicinity of ^{78}Ni from in-flight fission of ^{238}U [14]. β decay is an attractive alternative method for isomer identification as daughter nuclei can be populated in an excited state which, subsequently, decays to the ground state through one or more isomeric transitions. In the present paper,

*Corresponding author: chester@frib.msu.edu

†Present address: Lawrence Livermore National Laboratory, Livermore, California 94550.

‡Present address: Department of Chemistry, University of Kentucky, Lexington, Kentucky 40506.

a new isomeric transition was identified in ^{76}Zn following the β decay of ^{76}Cu. Previous experiments for ^{76}Zn built detailed level schemes [15,16] and determined $B(E2, 2_1^+ \rightarrow 0_1^+)$ and $B(E2, 4_1^+ \rightarrow 2_1^+)$ values [17,18] but did not report the presence of any isomeric states. The goal of this paper was to measure the properties of the newly identified isomeric state and place it within the level scheme of ^{76}Zn. Shell-model calculations, discussed in further detail in Sec. IV, suggest the isomeric state is a negative-parity state formed by the excitation of neutrons into the $0g_{9/2}$ orbital following β decay.

II. EXPERIMENTAL DETAILS

An experiment to study the properties of isomeric states near the $Z = 28$ and $N = 50$ shell gaps was performed at the National Superconducting Cyclotron Laboratory (NSCL). Radioactive ions were produced at the NSCL's Coupled Cyclotron Facility following the fragmentation of a 140-MeV/nucleon beam of ^{86}Kr on a 320-mg/cm^2 ^{9}Be target. Nuclei of interest, including ^{76}Cu, were separated using the A1900 fragment separator [19] at a momentum acceptance of 4.6% and delivered to an experimental end station consisting of three silicon detectors for particle identification and light ion rejection located approximately 1 m upstream of a $CeBr_3$ detector. Ions were implanted into the $CeBr_3$ scintillator (dimensions 51 mm × 51 mm × 3 mm) which was coupled to a position-sensitive photomultiplier tube (PSPMT) consisting of a single dynode and 256 anodes arranged in a 16 × 16 grid of 3-mm × 3-mm pixels [20]. Implanted ions were identified event by event with the ΔE-time-of-flight method similar to that described in Ref. [9] where beam particles are identified by examining the energy deposited in one of the silicon detectors and the time of flight between a position-sensitive scintillator located at the dispersive plane of the A1900 and one of the silicon detectors upstream of the $CeBr_3$ scintillator. A particle identification plot of the implanted ions is shown in Fig. 1. Correlations between β-decay events and implanted ions were established with a combination of spatial and temporal information recorded by the PSPMT.

β-delayed γ rays were measured by two ancillary detector systems which surrounded the implantation detector: An array of 16 HPGe clover detectors arranged in the squares of a rhombicuboctahedron frame (with two squares reserved for the beamline components) and an array of 15 $LaBr_3$ detectors [21], grouped in clusters of three and placed in the triangular openings between clovers. Twelve $LaBr_3$ detectors were installed upstream, and three were installed downstream of the center of the array. This configuration of $LaBr_3$ detectors was chosen to minimize the absorption of γ rays by beamline components downstream of the $CeBr_3$ implantation detector. The entire suite of detectors was instrumented with the NSCL Digital Data Acquisition System (DDAS) [22]. To achieve the best timing performance, the PSPMT dynode and $LaBr_3$ detectors were instrumented on a single 500-MHz, 14-bit analog-to-digital converter. DDAS was configured to capture pulse shape traces for the PSPMT dynode signal. The trace length was set to 400 ns with a 120-ns delay.

Dynode traces recorded by DDAS were analyzed to selectively identify isomeric transitions with a technique similar

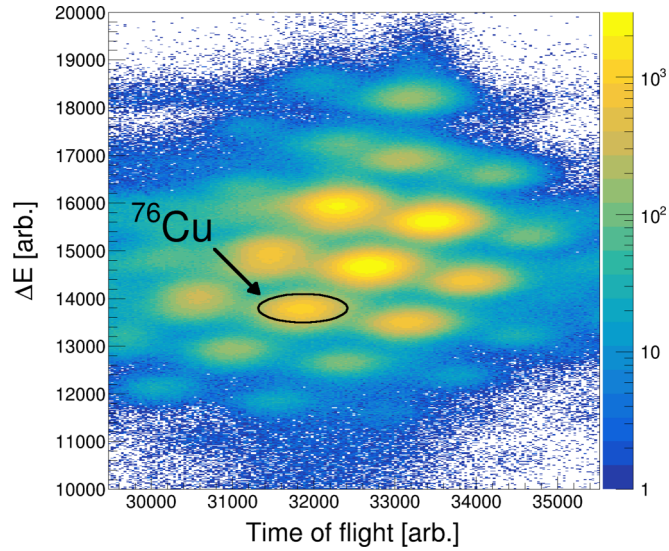

FIG. 1. Particle identification plot of ions implanted in the $CeBr_3$ detector. The ^{76}Cu ions of interest are circled.

to that described in Ref. [9]. The key experimental feature of a short-lived isomeric transition populated by β decay is the presence of two pulses recorded in the same dynode trace slightly separated in time, an example of which is shown in Fig. 2. The detector response was modeled using a logistic rise time and an exponential decay. Recorded traces were fit with both single- and two-model response functions along with a constant background term, and the best-fit parameters were determined using χ^2 minimization. Identification of double-pulse events was achieved by comparing the χ^2 values of the two fits. Traces where $\chi^2_{\text{single}}/\chi^2_{\text{double}} > 10$ were identified as

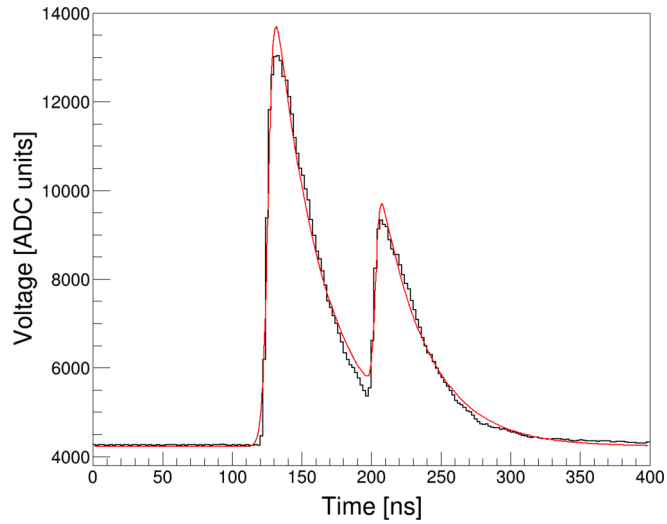

FIG. 2. An example of a double-pulse signal from the PSPMT dynode recorded by DDAS. These signals are characteristic of an isomeric transition populated following β decay. The best-fit detector response function described in Sec. II is shown in red. Features, such as the energies and the time difference between the two signals were determined from the fit.

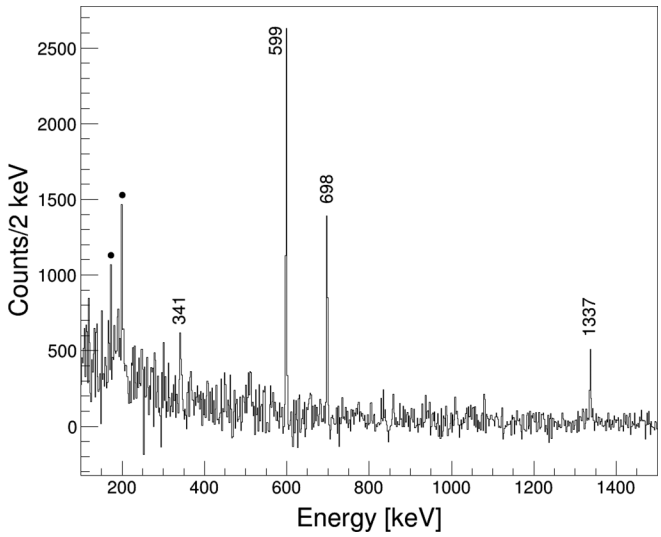

FIG. 3. Background-subtracted β-delayed γ rays detected within 3.2 s of a ^{76}Cu implant. The γ-ray transitions at 341, 599, 698, and 1337 keV are the strongest transitions observed in ^{76}Zn following the β decay of ^{76}Cu from Refs. [15,16]. The closed circles designate known transitions from ^{76}Ga, the granddaughter of ^{76}Cu, which are present due to ^{76}Zn β decay occurring within the 3.2-s correlation window.

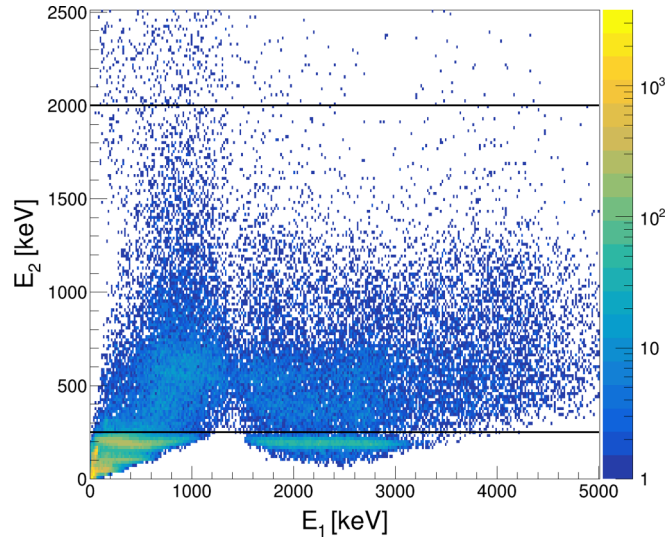

FIG. 4. The E_1-E_2 energy spectrum of double-pulse events separated by more than 20 ns identified following the procedure described in Sec. II. A gating region identified for further analysis is given by the horizontal black lines. For more details, refer to Sec. III.

double-pulse events; the result of the best-fit two-pulse model to an experimental trace is shown in Fig. 2. Features of the signals, such as their energies and the time difference between the two pulses were determined from the fit results for further analysis. In order to increase the selectivity of identifying double pulses, an additional requirement that the two pulses in the double-pulse fit were separated by, at least, 20 ns in time was imposed.

Excited states in ^{76}Zn were populated following the β decay of ^{76}Cu. β-delayed γ rays recorded in the two ancillary photon detector arrays up to 3.2 s following the detection of a ^{76}Cu ion were correlated with that implantation event. The 3.2-s time window for correlation was chosen to be approximately five ^{76}Cu ground-state half-lives [16]. The 341-, 599-, 698-, and 1337-keV γ rays previously observed in ^{76}Zn [15,16] were identified in the decay spectra correlated with ^{76}Cu implants through a combination of γ-γ coincidences and background-subtracted γ-ray spectra; an example of the latter is shown in Fig. 3.

III. ANALYSIS

The energy spectrum of double-pulse events identified using the procedure described in Sec. II is shown in Fig. 4 where the energy of the second pulse E_2 is plotted against the energy of the first E_1. Isomeric transitions following β decay leave a unique signature in this spectrum: A broad distribution of energies in E_1 arising from the β particle plus contributions from any prompt γ rays which scatter out of the $CeBr_3$ crystal, and a narrower distribution of energy in E_2 due to the isomeric transition. The narrower E_2 distribution may be broadened if the isomeric transition lies above a γ-ray cascade due to the addition of incomplete energy deposits from γ rays which scatter out of the $CeBr_3$ crystal.

Isomeric transitions can be assigned to a particular nucleus by examining their coincident γ-ray energy spectra. Coincident γ-ray energy spectra measured in the clover array and the $LaBr_3$ detectors for the gate on the double-pulse spectrum from Fig. 4 are shown in Fig. 5. The presence of the 341-, 599-, 698-, and 1337-keV transitions were used to place this isomer in ^{76}Zn. A previously unobserved γ ray at 2225.4(3) keV, shown in Fig. 6, was seen in coincidence with the ^{76}Zn double pulses with insufficient statistics to place in the level scheme. The half-life of the isomeric state, determined from the distribution of the time differences between the first and the second pulse was found to be 25.4(4) ns as shown in Fig. 7.

Timing information between γ rays detected in the $LaBr_3$ array, and the double-pulse signals measured in the PSPMT dynode were used to place the isomeric decay within the ^{76}Zn level scheme. A plot of the $LaBr_3$-PSPMT time difference for ^{76}Zn double-pulse events is shown in Fig. 8. Prompt γ rays which occur following the β decay of ^{76}Cu but prior to the isomeric transition are associated with the first of the two recorded pulses and, thus, have a time difference centered around $t_{LaBr_3} - t_{PSPMT} = 0$ because the first pulse defines the trigger time of the PSPMT dynode signal. Conversely, γ rays which depopulate the isomeric state are delayed due to the lifetime of the isomer and possess a time-difference $t_{LaBr_3} - t_{PSPMT} > 0$. A requirement that the two pulses in the recorded dynode trace are separated by, at least, 50 ns has been imposed in order to distinguish the peak centered at $t_{LaBr_3} - t_{PSPMT} = 0$ from the decay-curve distribution at $t_{LaBr_3} - t_{PSPMT} > 0$.

Coincident γ-ray spectra gated on the peak in Fig. 8 centered around $t_{LaBr_3} - t_{PSPMT} = 0$ and $t_{LaBr_3} - t_{PSPMT} > 50$ ns are shown in Fig. 9. The 341-keV transition, which is in

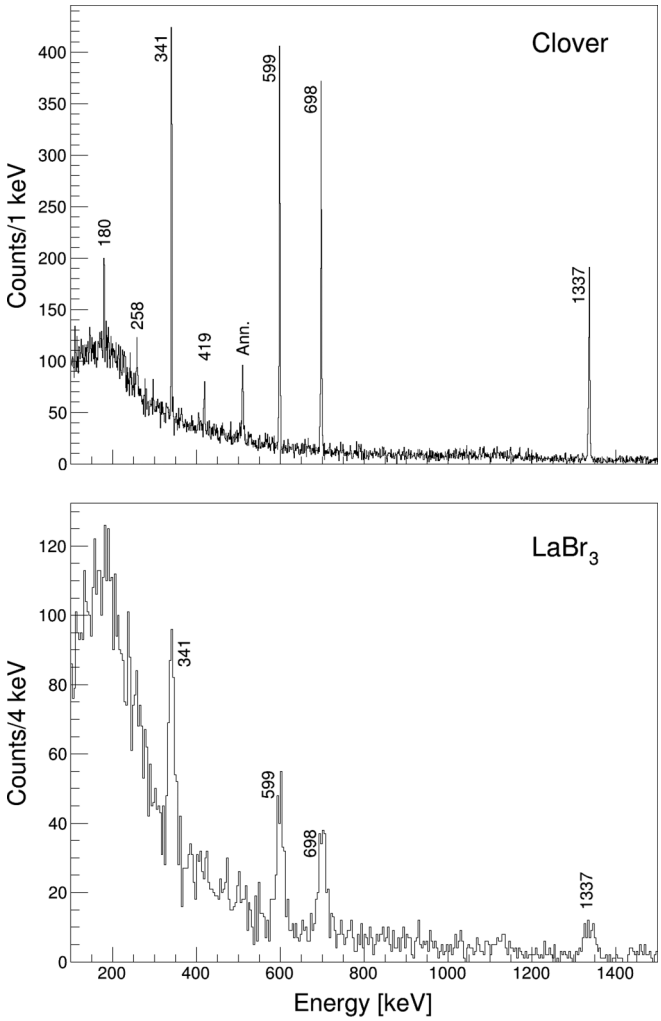

FIG. 5. γ rays measured with the clover array (top) and the $LaBr_3$ detectors (bottom) in coincidence with double pulses falling in the gating region shown in Fig. 4 where the coincident double pulses were separated by, at least, 20 ns in the dynode trace. The strongest transitions at 341, 599, 698, and 1337 keV have been observed previously in ^{76}Zn following ^{76}Cu β decay and were used to place the isomeric transition in ^{76}Zn.

coincidence with the peak centered around $t_{LaBr_3} - t_{PSPMT} = 0$ ns, must occur prior to the isomeric transition; the 599-, 698-, and 1337-keV γ rays are delayed and found in coincidence with the second pulse. This implies the isomeric state of interest is an intermediate state located below the state which is depopulated by the 341-keV γ ray.

The γ-ray cascade depopulating the isomeric state makes a precise energy measurement from this data difficult as scattered γ rays in the $CeBr_3$ crystal smear out the otherwise discrete energy which generates the second pulse signal as discussed previously. γ rays emitted following β decay travel some distance away from the decaying nucleus without interacting before depositing a fraction of their energy in, and scattering out of, the $CeBr_3$ crystal. This process manifests as a second distinct local maximum in the spatial distribution of anode energies. Many of the double-pulse events associated

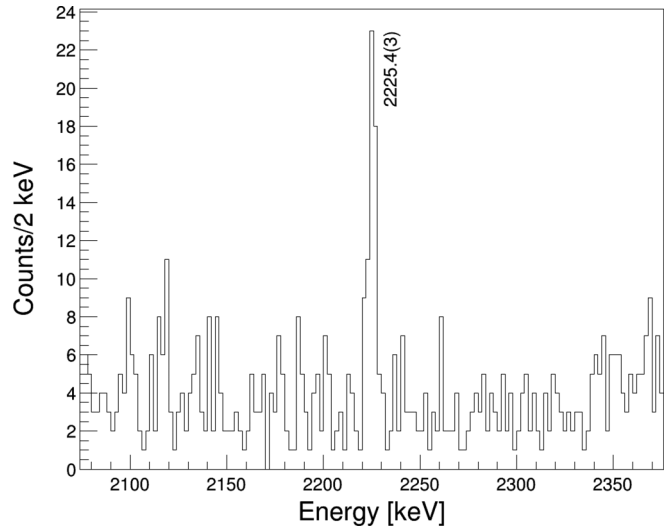

FIG. 6. Previously unobserved 2225.4(3)-keV γ-ray transition in coincidence with the double-pulse gate in the E_1-E_2 spectrum shown in Fig. 4. This γ ray is in coincidence with the isomeric transition in ^{76}Zn, however, it could not be placed in the level scheme due to insufficient statistics.

with the ^{76}Zn isomer have coincident anode energy spatial distributions containing two such local maxima as shown in Fig. 10, caused by these scattered γ rays. Observation of the ^{76}Zn isomer in the current paper but not in the previous

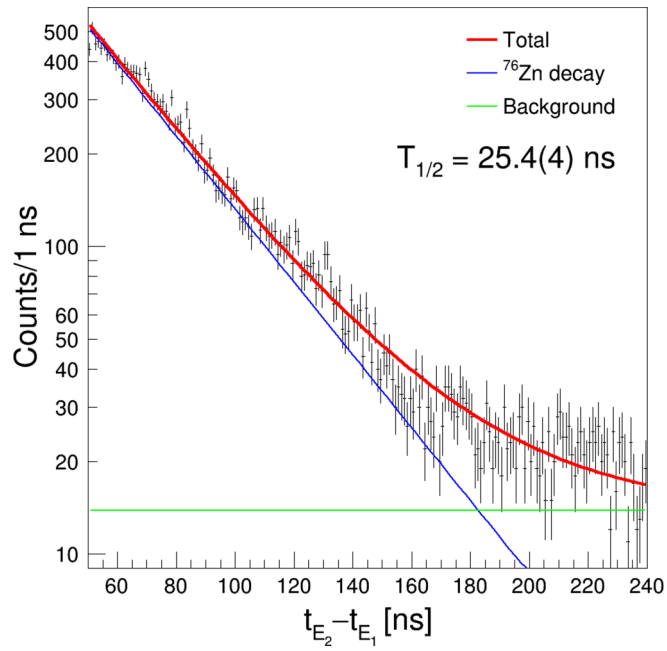

FIG. 7. Distribution of time differences between the first (E_1) and second (E_2) pulses determined from the fit parameters of the model detector response (black). The time difference was fit with an exponential decay plus a constant background (red) resulting in a measured half-life of 25.4(4) ns. The contributions to the total fit from the exponential decay and constant background are shown in blue and green, respectively.

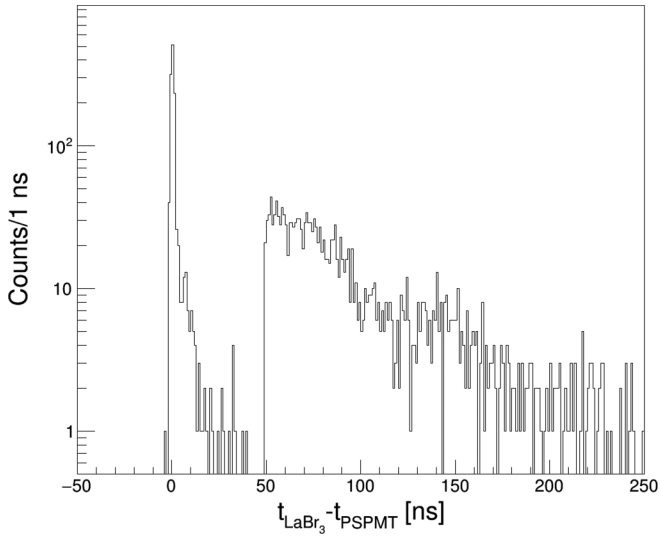

FIG. 8. The distribution of time differences between the $LaBr_3$ and PSPMT dynode signals for ^{76}Zn double-pulse events where the first and second pulses in the dynode trace are separated by, at least, 50 ns. Prompt γ rays which occur following the β decay of ^{76}Cu have a time difference centered around $t_{LaBr_3} - t_{PSPMT} = 0$ whereas γ rays which occur following the isomeric state are delayed and possess a time difference $t_{LaBr_3} - t_{PSPMT} > 0$.

in-flight fission-fragment study presented in Ref. [14] is likely due to its half-life of 25.4(4) ns being too short to survive the 600–700-ns flight path through the fragment separator prior to implantation at the experimental end station.

Taken together, the evidence suggests a short-lived isomeric state which decays by γ-ray emission, and further emits a cascade of γ rays to the ^{76}Zn ground state. No new γ rays were identified from the ^{76}Cu-correlated γ-γ coincidence matrix. As such, the most likely candidate for the isomeric state is the 2634-keV state which decays by emission of the 1337-keV γ ray, leading to the level scheme shown in Fig. 11 where the 2634-keV state is identified as isomeric. Efficiency-corrected γ-ray intensities of the observed transitions relative to the 1337-keV isomeric state are presented in Table I. The

TABLE I. Relative intensities of γ rays visible in the clover and $LaBr_3$ spectra shown in Fig. 5 normalized to the intensity of the 1337-keV isomeric transition. The reported intensities have been corrected to account for geometric and energy-dependent efficiencies of the detectors. Expected relative intensities based on Ref. [16] are shown in the third column. Uncertainties at 1σ are given in parentheses.

Energy (keV)	Clover	$LaBr_3$	Expected
180	0.12(2)		0.127(16)
258	0.10(3)		0.067(14)
341	0.68(5)	0.67(14)	0.53(5)
419	0.088(19)		0.113(15)
599	1.03(6)	1.0(2)	1.00(9)
698	0.99(6)	1.1(2)	1.00(9)
1337	1.00(7)	1.0(2)	1.00(9)

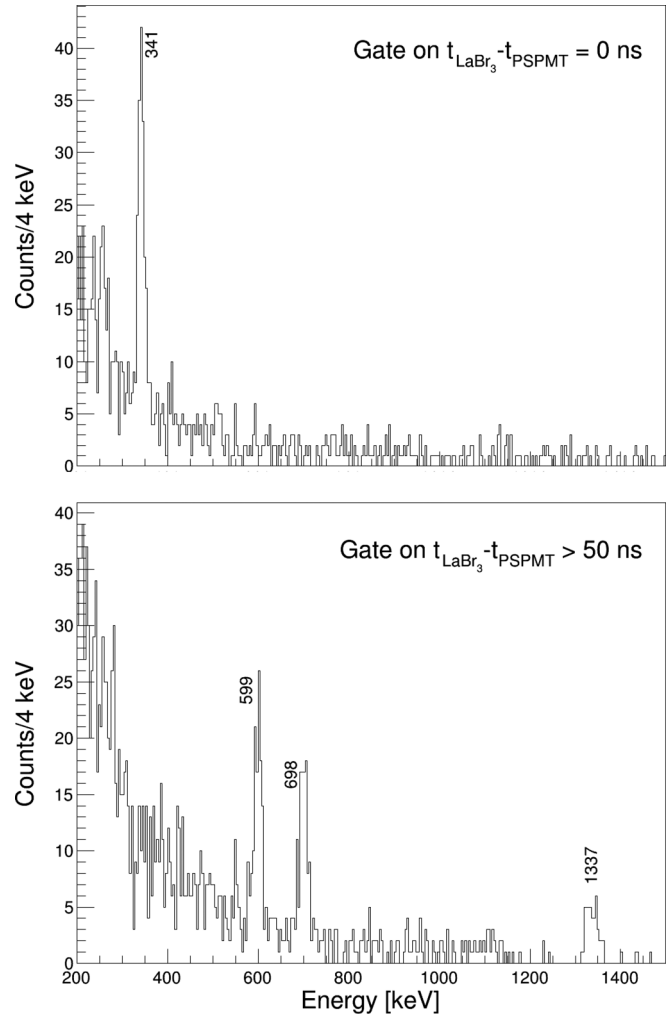

FIG. 9. $LaBr_3$ γ-ray spectra in coincidence with the double pulses in the gating region shown in Fig. 4 for the peak centered around $t_{LaBr_3} - t_{PSPMT} = 0$ ns (top) and $t_{LaBr_3} - t_{PSPMT} > 50$ ns (bottom). The coincidence relationships were used to place the isomeric state in the ^{76}Zn decay scheme below the 341-keV transition.

cause of the discrepancy between the measured and the expected relative intensities at 341 keV is not known.

IV. DISCUSSION

In Fig. 12 we compare the experimental decay scheme with those from three Hamiltonians that have been designed for protons and neutrons in the $(0f_{5/2}, 1p_{3/2}, 1p_{1/2}, 0g_{9/2})$ $(jj44)$ model space. The Hamiltonians and their origins are described in the Appendix of Ref. [23]. For the initial nucleus ^{76}Cu, these Hamiltonians predict that states with $J^\pi = (2, 3, 4, 6)^-$ all lie within 100 keV. Thus, all of these are possible ground state J^π and we expect to populate negative-parity states in ^{76}Zn.

To understand the origin of the isomer we first calculate $M1$ and $E2$ transition strengths. For positive-parity states, the longest lifetime comes from the first 8^+ state that has a half-life of 30–510 ps as predicted using the three Hamiltonians. Since the observed half-life is 25.4(4) ns, we

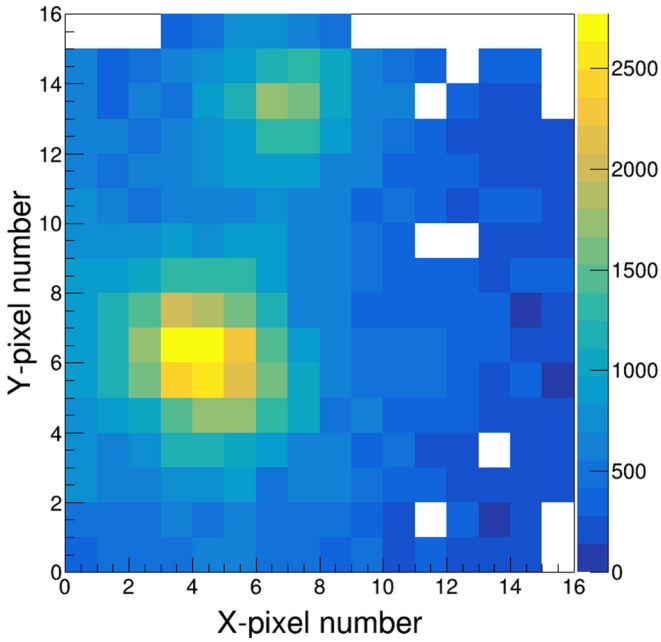

FIG. 10. An anode energy distribution for a double-pulse event attributed to the decay of the isomeric state in ^{76}Zn. The two discrete local maxima located at approximately (4,6) and (6,13) are generated by a β-decay electron followed by a γ-ray scattering out of the $CeBr_3$ crystal. This suggests that the isomeric state lies above a γ-ray cascade and explains the broadened E_2 distribution shown in Fig. 4.

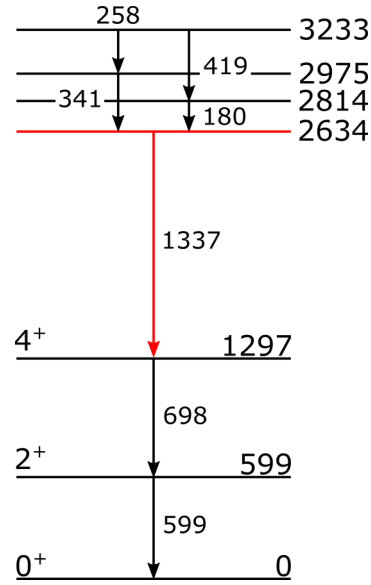

FIG. 11. Level scheme showing the states of interest and observed transitions in ^{76}Zn for the current paper with energies given in keV. The assignment of 2^+ and 4^+ for the first two excited states is taken from Refs. [17,18]. Spins and parities could not be assigned to other states observed in the present paper. The 2634-keV state which has been newly identified as isomeric in this paper is shown in red.

therefore turn to $E1$ and $M2$ transition strengths from negative parity to lower-lying, positive-parity states. In this model space all $E1$ transitions are forbidden. For pure $M2$ transitions, the lifetimes of the lowest-energy negative-parity states are on the order of a few microseconds, which is much longer than observed. All higher multipolarities would be expected to have even longer half-lives, thus, an $E1$ transition is the most plausible candidate. For the $E1$ γ decay we start by using the most likely value of 10^{-4} e^2fm^2 observed for other $E1$ transitions in the 1979 evaluation of this mass region, see Fig. 1 in Ref. [24]; the longest lifetime for the negative-parity states in this case was about 15 ps. The only way to produce a half-life comparable to experiment is to use $B(E1) = 10^{-8}$ e^2fm^2 where we obtain the lifetimes shown in Fig. 12. This is an order of magnitude smaller than the weakest $E1$ strength observed in this mass region in the 1979 compilation. All three Hamiltonians predict lower-energy transitions feeding the $E1$ isomer.

A recent hyperfine-structure study determined the ground-state spin of the ^{76}Cu parent to be $J = 3$ [25], which is consistent with previous β-decay studies that suggested a $J = (3, 4)$ ground-state spin [16] and with the calculations presented here. In the case of a $J^\pi = 3^-$ ground state for ^{76}Cu, a significant population of negative-parity states with $J = 2$ to $J = 4$ in ^{76}Zn would be expected. The shell-model calculations predict a number of negative-parity states with energies greater than 2600 keV which feed negative-parity isomeric states with $J = 4$–6 and half-lives ranging from approximately 2–30 ns. States with $J^\pi = 3^-$ are also present in the calculations; the lowest-lying 3^- states have half-lives

TABLE II. Proton and neutron occupancy numbers of negative-parity isomeric states with $J = 4$–6 and $T_{1/2} \approx 2$–30 ns from the shell-model calculations discussed in this paper using a $B(E1)$ value of 10^{-8} e^2fm^2. The states of interest involve the excitation of a neutron from either the $1p_{1/2}$ ($J = 4, 5$) or $0f_{5/2}$ ($J = 6$) orbitals. For the 6^- states, a larger occupancy of the $\pi 1p_{3/2}$ and $\pi 1p_{1/2}$ orbitals is expected relative to the 4^- and 5^- states.

Hamiltonian	Energy (keV)	J^π	$\pi 0f_{5/2}$	$\pi 1p_{3/2}$	$\pi 1p_{1/2}$	$\pi 0g_{9/2}$	$\nu 0f_{5/2}$	$\nu 1p_{3/2}$	$\nu 1p_{1/2}$	$\nu 0g_{9/2}$
jj44b	2799	6^-	1.03	0.61	0.31	0.05	4.98	3.95	1.96	7.10
	2850	4^-	1.38	0.33	0.23	0.06	5.91	3.76	1.22	7.11
	2893	5^-	1.43	0.34	0.17	0.06	5.77	3.77	1.23	7.23
jj44c	2650	6^-	1.07	0.58	0.30	0.04	4.98	3.96	1.97	7.09
	2703	4^-	1.38	0.34	0.23	0.05	5.92	3.83	1.15	7.11
JUN45	2891	5^-	1.26	0.54	0.13	0.08	5.82	3.85	1.12	7.22
	2974	4^-	1.25	0.51	0.17	0.07	5.87	3.88	1.09	7.15

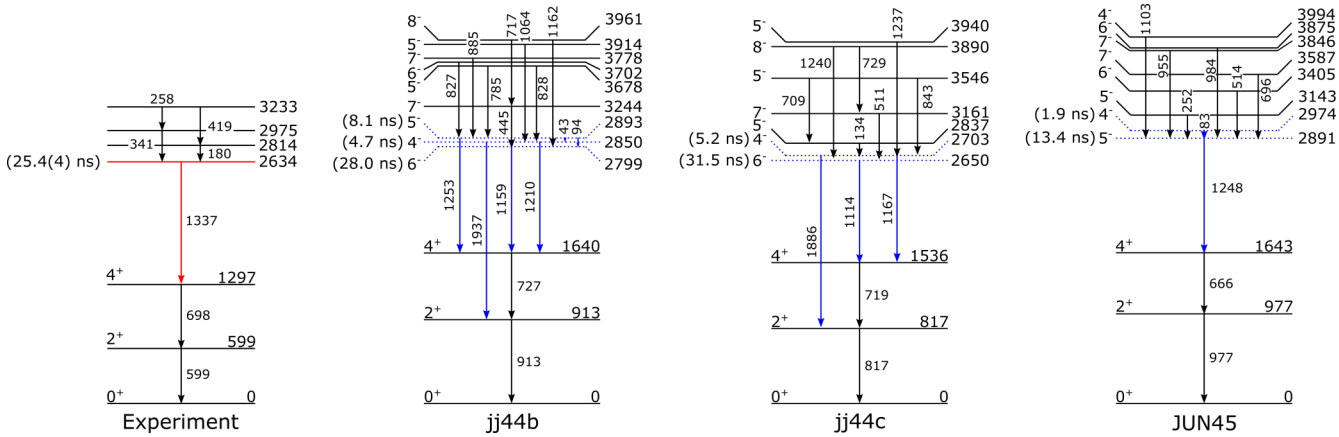

FIG. 12. Comparison between the experimentally observed level scheme and partial level schemes determined using the shell-model calculations and their associated Hamiltonians described in Sec. IV. The experimental level scheme is presented the same as in Fig. 11. Negative-parity states with half-lives longer than 1 ns from the shell-model calculations are shown using blue dotted lines; their depopulating transitions are also shown in blue. Half-lives of isomeric states assuming a $B(E1)$ value of 10^{-8} $e^2\text{fm}^2$ are given in parentheses to the left of the level spin and parity. Levels up to 4 MeV and γ rays with branching ratios $> 20\%$ which decay through the yrast 4-2-0 cascade are shown for the calculations.

ranging from approximately 130–220 ps, which is two orders of magnitude smaller than the observed half-life of the 2634-keV state. The predicted $J = 4$–6 isomeric states involve the excitation of a neutron into the $0g_{9/2}$ orbital. In the case of the 4^- and 5^- states the excitation occurs primarily from $1p_{1/2}$ to $0g_{9/2}$, whereas for the 6^- states, the excitation is primarily $0f_{5/2}$ to $0g_{9/2}$. The 6^- states also have a larger occupancy of the $\pi 1p_{3/2}$ and $\pi 1p_{1/2}$ orbitals relative to the 4^- and 5^- states. Occupancy numbers for the isomeric states of interest are given in Table II.

The presence of negative-parity isomeric states in the calculations with half-lives and energies comparable to the experimental data offer an explanation for the observed decay pattern. The 2634-keV isomeric state is populated by some combination of direct feeding from the ^{76}Cu parent plus β decay into negative-parity states in ^{76}Zn which decay by γ-ray emission and feed the negative-parity isomer. The isomeric state, subsequently, decays by emission of a 1337-keV γ ray followed by the 698–599-keV cascade to the ^{76}Zn ground state, which is in good agreement with all of the calculations presented in this paper. More knowledge of the spins and parities of excited states in ^{76}Zn would allow for more detailed conclusions to be drawn between theory and experiment.

V. CONCLUSIONS

The 2634-keV state in ^{76}Zn, populated following the β decay of ^{76}Cu, has been identified as isomeric with a half-life of 25.4(4) ns. Shell-model calculations were performed which identified candidate negative-parity isomeric states arising from neutron excitations into the $0g_{9/2}$ orbital. The presence of the isomer indicates that the $E1$ transition strength involved in the decay is very weak, about 10^{-8} $e^2\text{fm}^2$, which is an order of magnitude weaker than any of the transition strengths in this mass region reported in Ref. [24]. Resolving the ambiguity of the spin of the observed isomeric state as well as the identification and characterization of other short-lived isomeric states in the region will shed light on nuclear shell structure near doubly magic ^{78}Ni. The result also demonstrates the value of this experimental technique for identifying isomeric states populated following β decay and is a promising method for future radioactive ion beam experiments.

Note added in proof. A recent Caen Ph.D. thesis [26] indicates the presence of an isomeric level in ^{76}Cu at 64 keV. This possible high-spin β-decaying isomeric state has been observed in Ref. [15] and Ref. [26], though its exact spin and feeding of states in ^{76}Zn is unknown; the proposed isomeric state was not observed in Ref. [16].

ACKNOWLEDGMENTS

This work was supported by the US Department of Energy (DOE) National Nuclear Security Administration Grant No. DOE-DE-NA0003906, the Nuclear Science and Security Consortium under Award No. DE-NA0003180, and the DOE Office of Nuclear Physics under Grants No. DE-SC0020451 and No. DE-AC02-06CH11357 (Argonne National Laboratory). Additional support was provided under the auspices of the DOE by the Lawrence Livermore National Laboratory (LLNL) under Contract No. DE-AC52-07NA27344 and the Laboratory Directed Research and Development (LDRD) Program at LLNL under Project No. 21-FS-011. Further support was provided by the National Science Foundation (NSF) Grant No. PHY-1848177 (CAREER) (Mississippi State University) and NSF Grant No. PHY-1811855.

[1] R. Grzywacz, R. Béraud, C. Borcea, A. Emsallem, M. Glogowski, H. Grawe, D. Guillemaud-Mueller, M. Hjorth-Jensen, M. Houry, M. Lewitowicz, A. C. Mueller, A. Nowak, A. Płochocki, M. Pfützner, K. Rykaczewski, M. G. Saint-Laurent,

J. E. Sauvestre, M. Schaefer, O. Sorlin, J. Szerypo *et al.*, Phys. Rev. Lett. **81**, 766 (1998).

[2] C. Mazzocchi, R. Grzywacz, J. C. Batchelder, C. R. Bingham, D. Fong, J. H. Hamilton, J. K. Hwang, M. Karny, W. Krolas, S. N. Liddick, A. F. Lisetskiy, A. C. Morton, P. F. Mantica, W. F. Mueller, K. P. Rykaczewski, M. Steiner, A. Stolz, and J. A. Winger, Phys. Lett. B **622**, 45 (2005).

[3] J. M. Daugas, R. Grzywacz, M. Lewitowicz, L. Achouri, J. C. Angélique, D. Baiborodin, K. Bennaceur, R. Bentida, R. Béraud, C. Borcea, C. Bingham, W. N. Catford, A. Emsallem, G. de France, H. Grawe, K. L. Jones, R. C. Lemmon, M. J. Lopez Jimenez, F. Nowacki, F. de Oliveira Santos *et al.*, Phys. Lett. B **476**, 213 (2000).

[4] A. I. Morales, G. Benzoni, H. Watanabe, G. de Angelis, S. Nishimura, L. Coraggio, A. Gargano, N. Itaco, T. Otsuka, Y. Tsunoda, P. Van Isacker, F. Browne, R. Daido, P. Doornenbal, Y. Fang, G. Lorusso, Z. Patel, S. Rice, L. Sinclair, P.-A. Söderström *et al.*, Phys. Lett. B **781**, 706 (2018).

[5] A. F. Lisetskiy, B. A. Brown, M. Horoi, and H. Grawe, Phys. Rev. C **70**, 044314 (2004).

[6] D. Pauwels, O. Ivanov, N. Bree, J. Büscher, T. E. Cocolios, J. Gentens, M. Huyse, A. Korgul, Y. Kudryavtsev, R. Raabe, M. Sawicka, I. Stefanescu, J. Van de Walle, P. Van den Bergh, P. Van Duppen, and W. B. Walters, Phys. Rev. C **78**, 041307(R) (2008).

[7] J. Van Roosbroeck, C. Guénaut, G. Audi, D. Beck, K. Blaum, G. Bollen, J. Cederkall, P. Delahaye, A. De Maesschalck, H. De Witte, D. Fedorov, V. N. Fedoseyev, S. Franchoo, H. O. U. Fynbo, M. Górska, F. Herfurth, K. Heyde, M. Huyse, A. Kellerbauer, H.-J. Kluge *et al.*, Phys. Rev. Lett. **92**, 112501 (2004).

[8] M. P. Carpenter, R. V. F. Janssens, and S. Zhu, Phys. Rev. C **87**, 041305(R) (2013).

[9] S. Suchyta, S. N. Liddick, C. J. Chiara, W. B. Walters, M. P. Carpenter, H. L. Crawford, G. F. Grinyer, G. Gürdal, A. Klose, E. A. McCutchan, J. Pereira, and S. Zhu, Phys. Rev. C **89**, 067303 (2014).

[10] C. J. Prokop, B. P. Crider, S. N. Liddick, A. D. Ayangeakaa, M. P. Carpenter, J. J. Carroll, J. Chen, C. J. Chiara, H. M. David, A. C. Dombos, S. Go, J. Harker, R. V. F. Janssens, N. Larson, T. Lauritsen, R. Lewis, S. J. Quinn, F. Recchia, D. Seweryniak, A. Spyrou *et al.*, Phys. Rev. C **92**, 061302(R) (2015).

[11] C. J. Chiara, D. Weisshaar, R. V. F. Janssens, Y. Tsunoda, T. Otsuka, J. L. Harker, W. B. Walters, F. Recchia, M. Albers, M. Alcorta, V. M. Bader, T. Baugher, D. Bazin, J. S. Berryman, P. F. Bertone, C. M. Campbell, M. P. Carpenter, J. Chen, H. L. Crawford, H. M. David *et al.*, Phys. Rev. C **91**, 044309 (2015).

[12] B. P. Crider, C. J. Prokop, S. N. Liddick, M. Al-Shudifat, A. D. Ayangeakaa, M. P. Carpenter, J. J. Carroll, J. Chen, C. J. Chiara, H. M. David, A. C. Dombos, S. Go, R. Grzywacz, J. Harker, R. V. F. Janssens, N. Larson, T. Lauritsen, R. Lewis, S. J. Quinn, F. Recchia *et al.*, Phys. Lett. B **763**, 108 (2016).

[13] S. N. Liddick, S. Suchyta, B. Abromeit, A. Ayres, A. Bey, C. R. Bingham, M. Bolla, M. P. Carpenter, L. Cartegni, C. J. Chiara, H. L. Crawford, I. G. Darby, R. Grzywacz, G. Gürdal, S. Ilyushkin, N. Larson, M. Madurga, E. A. McCutchan, D. Miller, S. Padgett *et al.*, Phys. Rev. C **84**, 061305(R) (2011).

[14] D. Kameda, T. Kubo, T. Ohnishi, K. Kusaka, A. Yoshida, K. Yoshida, M. Ohtake, N. Fukuda, H. Takeda, K. Tanaka, N. Inabe, Y. Yanagisawa, Y. Gono, H. Watanabe, H. Otsu, H. Baba, T. Ichihara, Y. Yamaguchi, M. Takechi, S. Nishimura *et al.*, Phys. Rev. C **86**, 054319 (2012).

[15] J. A. Winger, J. C. Hill, F. K. Wohn, E. K. Warburton, R. L. Gill, A. Piotrowski, R. B. Schuhmann, and D. S. Brenner, Phys. Rev. C **42**, 954 (1990).

[16] J. Van Roosbroeck, H. De Witte, M. Gorska, M. Huyse, K. Kruglov, D. Pauwels, J.-C. Thomas, K. Van de Vel, P. Van Duppen, S. Franchoo, J. Cederkall, V. N. Fedoseyev, H. Fynbo, U. Georg, O. Jonsson, U. Köster, L. Weissman, W. F. Mueller, V. I. Mishin, D. Fedorov *et al.*, Phys. Rev. C **71**, 054307 (2005).

[17] J. Van de Walle, F. Aksouh, F. Ames, T. Behrens, V. Bildstein, A. Blazhev, J. Cederkäll, E. Clément, T. E. Cocolios, T. Davinson, P. Delahaye, J. Eberth, A. Ekström, D. V. Fedorov, V. N. Fedosseev, L. M. Fraile, S. Franchoo, R. Gernhauser, G. Georgiev, D. Habs *et al.*, Phys. Rev. Lett. **99**, 142501 (2007).

[18] J. Van de Walle, F. Aksouh, T. Behrens, V. Bildstein, A. Blazhev, J. Cederkäll, E. Clément, T. E. Cocolios, T. Davinson, P. Delahaye, J. Eberth, A. Ekström, D. V. Fedorov, V. N. Fedosseev, L. M. Fraile, S. Franchoo, R. Gernhauser, G. Georgiev, D. Habs, K. Heyde *et al.*, Phys. Rev. C **79**, 014309 (2009).

[19] D. J. Morrissey, B. M. Sherrill, M. Steiner, A. Stolz, and I. Wiedenhoever, Nucl. Instrum. Methods Phys. Res., Sect. B **204**, 90 (2003).

[20] Data Sheet, *Flat panel type mutlianode PMT assembly H13700 series*, Hamamatsu Photonics KK, 314-5, Shimokanzo, Iwata City, Shizuoka Pref., 438-0193, Japan (2020), retrieved from: https://www.hamamatsu.com/resources/pdf/etd/H13700_TPMH1370E.pdf. Accessed 2 April 2021.

[21] B. Longfellow, P. C. Bender, J. Belarge, A. Gade, and D. Weisshaar, Nucl. Instrum. Methods Phys. Res., Sect. A **916**, 141 (2019).

[22] C. J. Prokop, S. N. Liddick, B. L. Abromeit, A. T. Chemey, N. R. Larson, S. Suchyta, and J. R. Tompkins, Nucl. Instrum. Methods Phys. Res., Sect. A **741**, 163 (2014).

[23] S. Mukhopadhyay, B. P. Crider, B. A. Brown, S. F. Ashley, A. Chakraborty, A. Kumar, M. T. McEllistrem, E. E. Peters, F. M. Prados-Estévez, and S. W. Yates, Phys. Rev. C **95**, 014327 (2017).

[24] P. M. Endt, At. Data Nucl. Data Tables **23**, 547 (1979).

[25] R. P. de Groote, J. Billowes, C. L. Binnersley, M. L. Bissell, T. E. Cocolios, T. Day Goodacre, G. J. Farooq-Smith, D. V. Fedorov, K. T. Flanagan, S. Franchoo, R. F. Garcia Ruiz, A. Koszorús, K. M. Lynch, G. Neyens, F. Nowacki, T. Otsuka, S. Rothe, H. H. Stroke, Y. Tsunoda, A. R. Vernon *et al.*, Phys. Rev. C **96**, 041302(R) (2017).

[26] S. Giraud, Ph.D. thesis, Normandie Universite, 2021, https://tel.archives-ouvertes.fr/tel-03354941/document.